

**A bigger splat: The catastrophic geology of a 1.2-b.y.-year old terrestrial megaclast,
NW Scotland**

Killingback, Z.¹, Holdsworth, R.E.¹, Walker, R.J.², Nielsen, S.¹, Dempsey, E.³ & Hardman, K.^{1,3}

1 = Department of Earth Sciences, Durham University, UK.

2 = School of Geography, Geology, and the Environment, University of Leicester, UK.

3 = Department of Geography, Environment and Earth Sciences, University of Hull, UK.

Supplementary Materials

Appendix I – Contextual geological map and stratum contour construction on base of Clachtoll Megablock

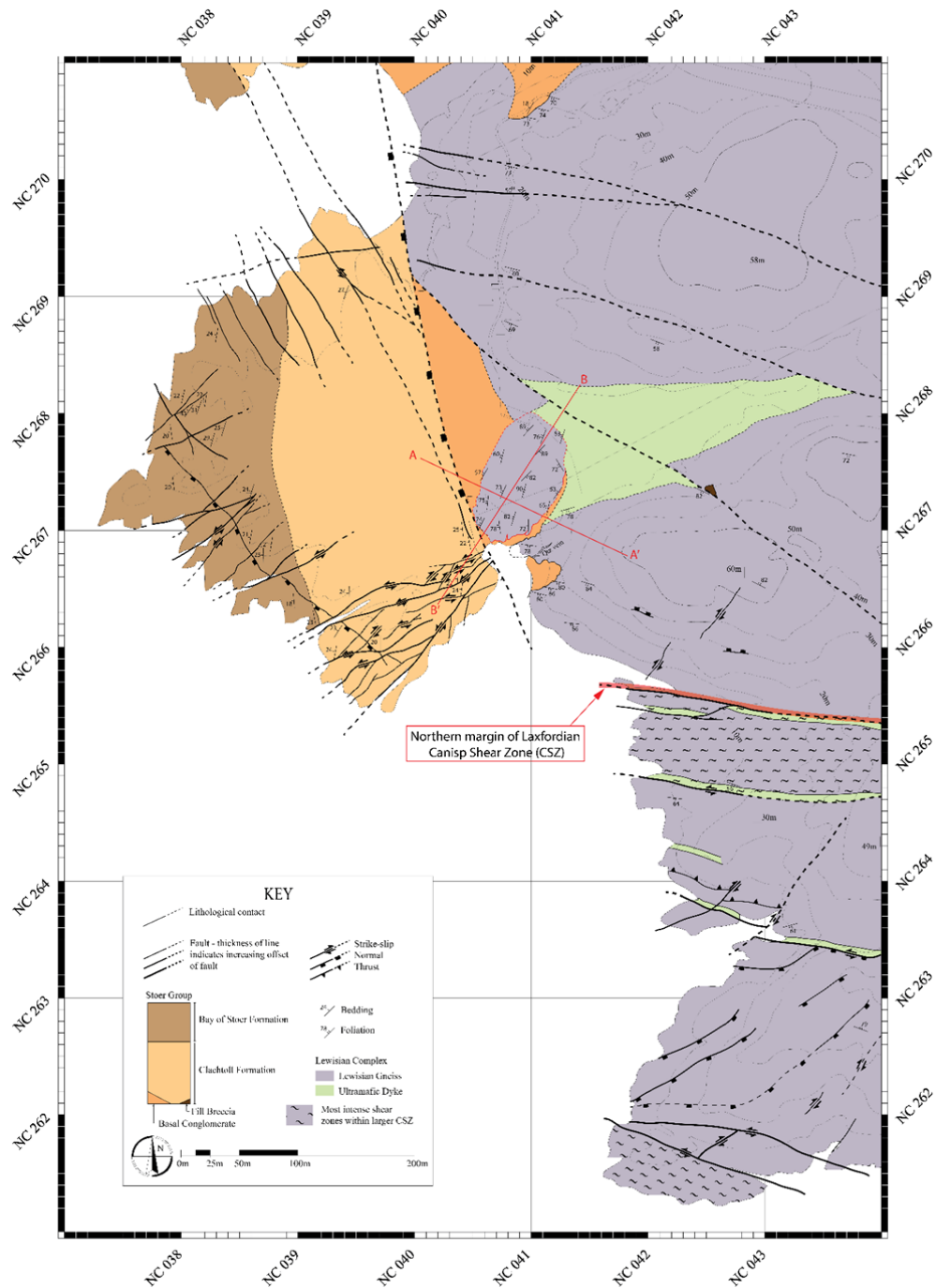


Figure I.1) Larger context map of geology. Red lines marked A-A' and B-B' denote the lines of section used to construct the cross sections found in Fig. 1c of main paper. Location of northern margin of Laxfordian CSZ after Attfield (1987).

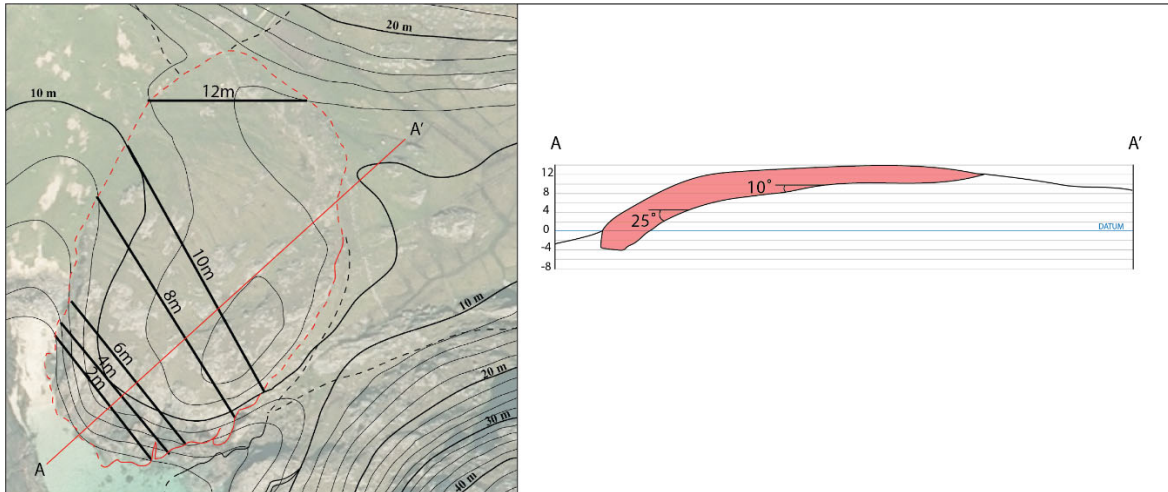


Figure II.2) Image on left shows structural contours (solid black lines) drawn on the basal contact of the Clachtoll Megablock. The topographic contours taken from the DEM are 2m spacing. Image on left shows cross-section view A-A'.

Appendix II – Additional field photographs of Group B and C sediment-filled fractures

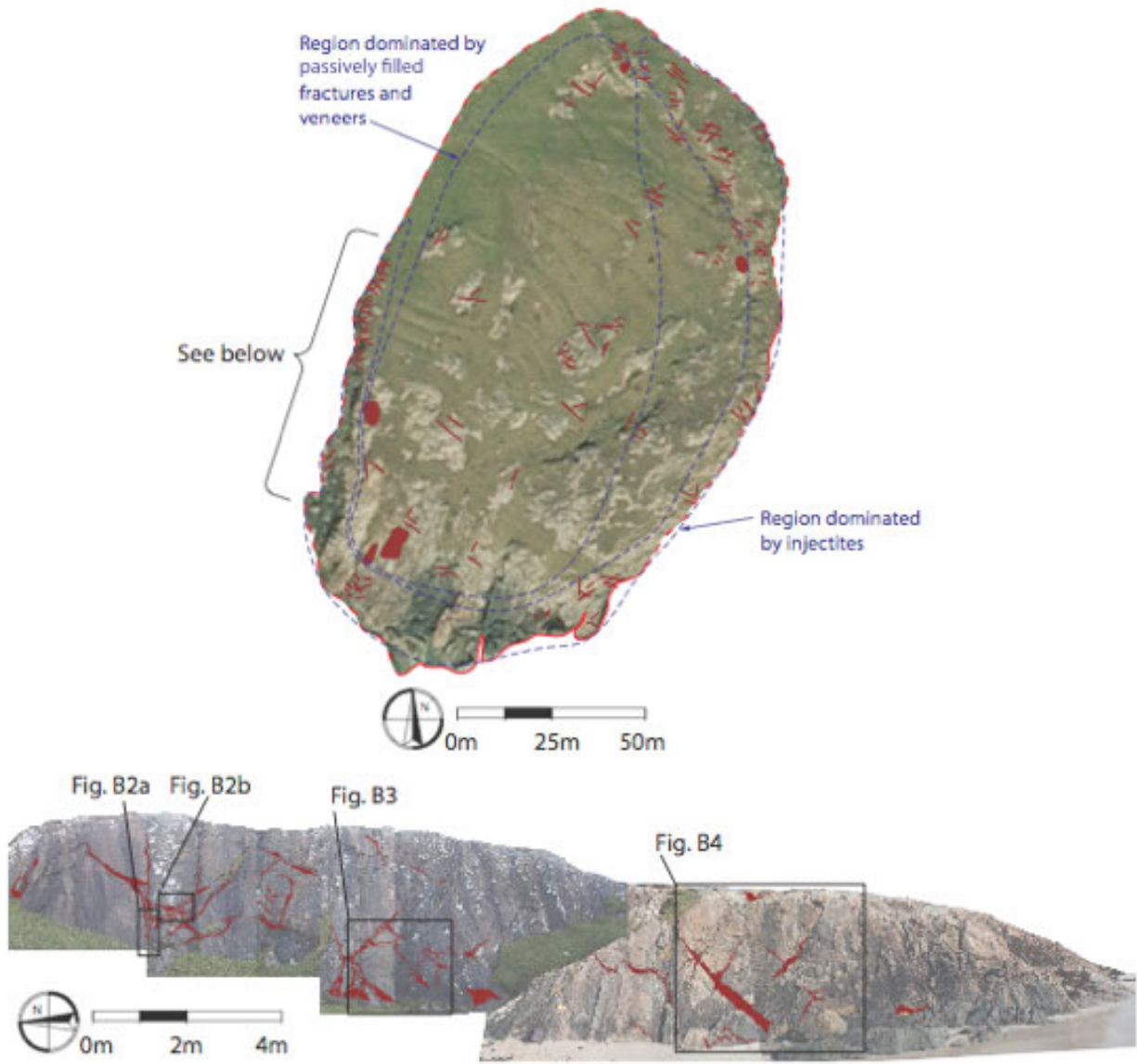


Figure II.1) Map of sediment-filled fractures and location of Figs B2-4.

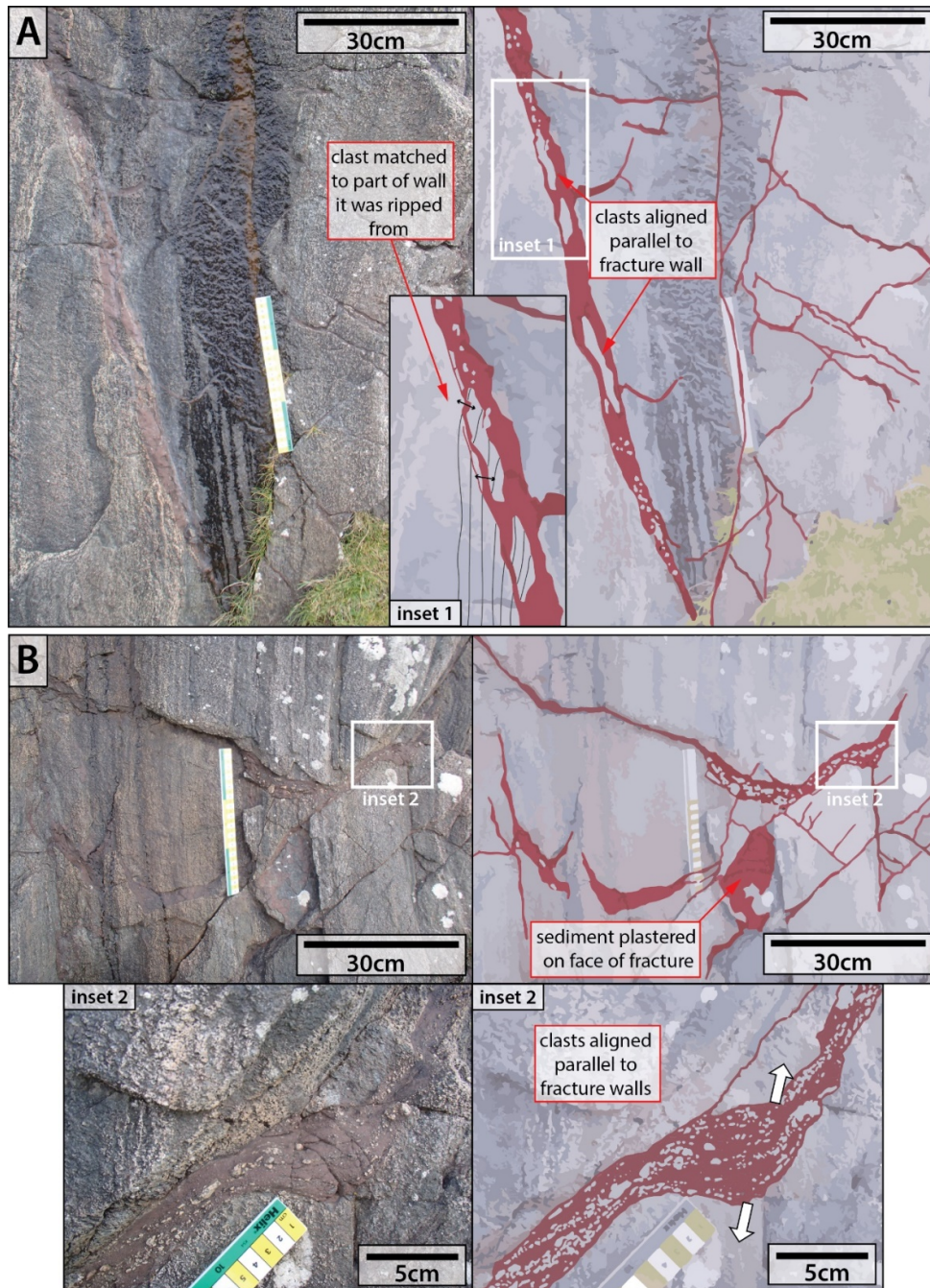


Figure II.2) Forcefully intruded Group B sediment filled fractures on the west side of the Clachtoll Megablock. (A) Fracture containing stopped wall raft, (B) Fracture wall parallel banding with sediment fill.

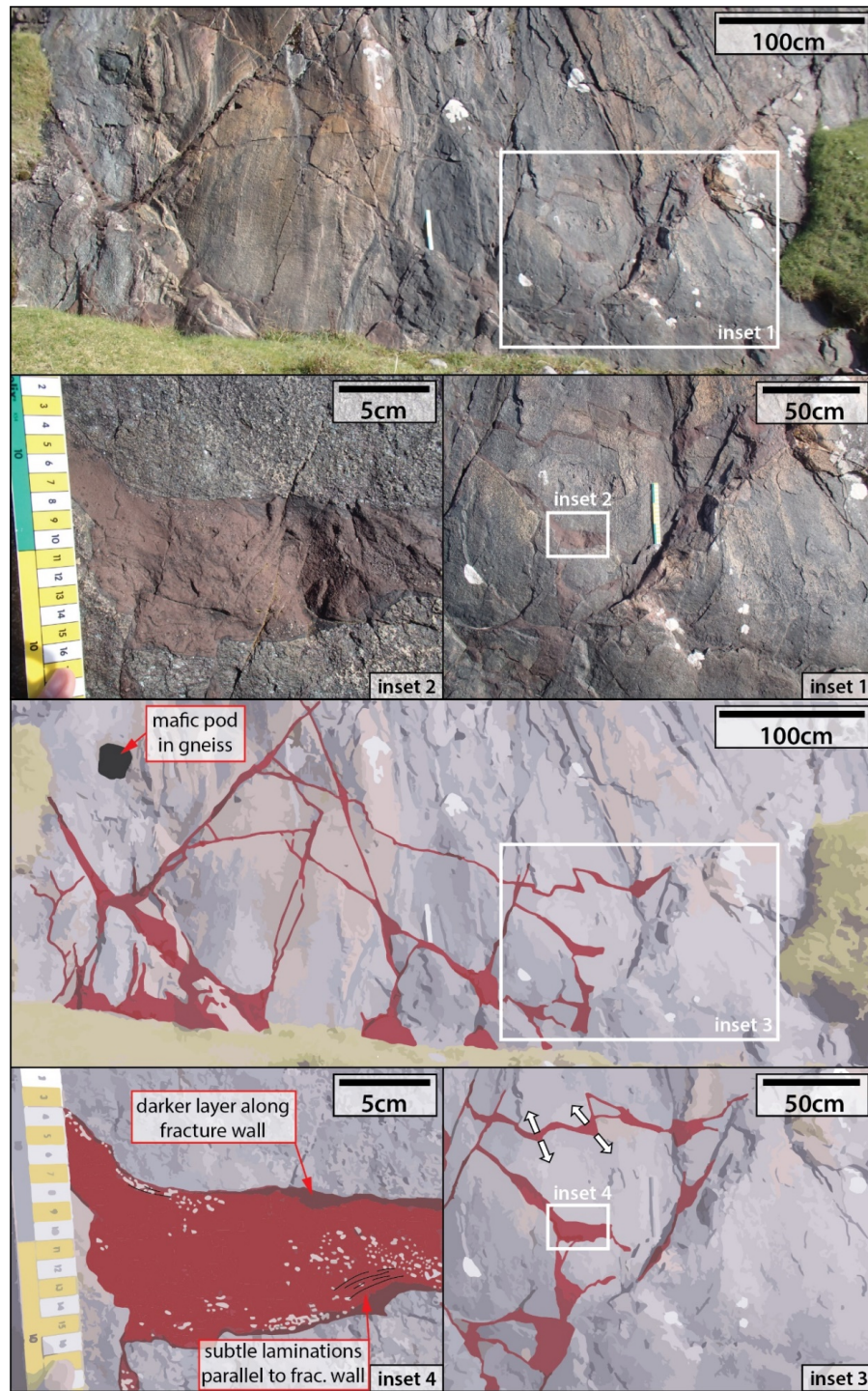


Figure II.3) Forcefully intruded Group B type sediment filled fractures on the west side of the Clachtoll Megablock, showing complex networks and occasional laminations parallel to fracture wall. Note that the central lower image is Fig 3b in the main paper.

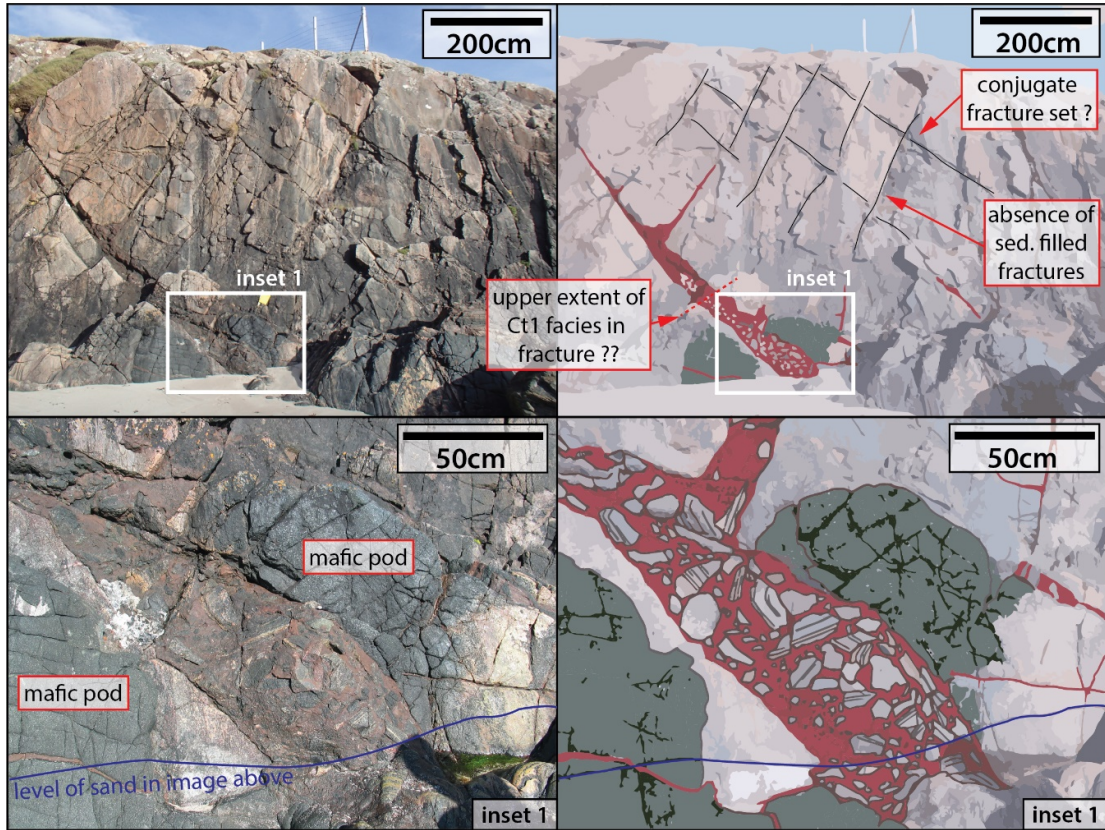


Figure II.4) Wide aperture Group C type fracture on the west side of the Clachtoll megablock with several smaller Group C type injections coming off it. These fractures appear to follow a set of (apparently) conjugate, non-sediment filled fractures. Note that the upper right image is Fig.3c in the main paper.

Appendix III – The solid collision equations

I.1. Model/hypothesis

Our hypothesis is that the Clachtoll Megablock (CM) represents a fallen block that impacted fluid-laden sediment causing a transient, dynamic pressure surge of that fluid and the consequent hydrofracturing of the overlying block. The impact-generated stress waves would also have reached the top surface of the block, generating tensile fractures there, but to a lesser extent than at the base (as observed), where the additional fluid pressure aided the tensile fracturing and the forceful injection of wet sediment. The top fractures were later gravitationally filled by sediment as the block was progressively buried (see Fig. 4c in the main paper). Stratum contours (Appendix I) suggest that the block has a flat or gently curvilinear base.

The premise that we wish to explore is that impact led to injection of wet sediments into the fallen block of gneiss. This is dependent on the impact generating sufficient overpressure to overcome the tensile strength of the fallen block. If this process is mechanically feasible, we then wish to determine the minimum height from which the block had to fall to achieve this and whether this is geologically plausible for the terrestrial Stoer Group basin setting.

II.2. Problem outline and assumptions

In order to simplify the problem to allow numerical calculations to be undertaken, several simplifying assumptions are necessary. Firstly, we assume a simple, vertical free fall of the block, neglecting rotations or translations that have occurred in addition to the vertical displacement. We also assume the block itself to be homogeneous. Finally, we assume a flat impact of the block, where all of the underlying surface impacts the ground at the same time.

Impact consequences can be analysed globally (i.e. in terms of the conversion of kinetic energy from whole colliding mass) or locally (i.e. in terms of waves generated in the vicinity of the object boundaries immediately after impact). In terms of dynamic fracturing, initiation and propagation will occur at a local scale within short time intervals, in the immediate vicinity of the impact surface. Thus the second approach is applied here.

Usually such an analysis is used in cases where both objects are solid elastic and have similar impedance. Here we extend the analysis to collision of media with contrasting properties – elastic stress wave on the impacting object and acoustic pressure waves on the target medium. Since the

sandstone matrix of the breccia-conglomerate is assumed to be saturated – as it has just been deposited - we describe the propagation of an acoustic wave using the properties of water incompressibility and density.

At the time of impact, we can reduce analysis to one dimension – considering any point where the waves diffracted from the outer borders of the object, and propagating laterally, have not yet arrived. For a megablock of linear dimension 15 m, the centre of the impact surface will be reached by lateral waves only at times of the order of ≈ 1 ms after impact. Later developments of the stress wavefield will be more complex, but after about 1 ms, dynamic tension fractures will already have nucleated and propagated up to a few metres within the boulder (Fig. 4c, main paper).

Our analysis also considers sections of the impacting object whose surface is parallel to the ground, and we assume that the ground is relatively planar. Under those assumptions, the elastic strain within the block, immediately after impact, will be reduced to shortening parallel to the vertical (fall) direction. The Poisson expansion is suppressed during this initial one-dimensional (vertical) compression, therefore there is no lateral dilation. This results in an additional compressive stress term which will work against the tensile fracture, and this should be accounted for in the calculation. Both stress and pressure waves, within the impacting megablock and underlying saturated sediment, respectively, will propagate away from the impact surface at a velocity equivalent to typical P-waves in the rock (ca. 5000 m/s) and acoustic waves in water (ca. 1500 m/s).

III.3. Equations describing the solid collision

We start our analysis with the classic problem of the collision between two elastic solid bodies of identical impedance (Fig. III.1, upper diagram). In the case of a rockfall, this may equate to a rock boulder falling on a solid rock surface of the same composition.

It is known that the initial wave due to the impact will produce a constant displacement gradient

$$\frac{\partial u}{\partial z} = \frac{-v_b}{V_p} \tag{C1}$$

in the target object, within the thickness reached by the propagating wave, i.e., $z_c = V_p t$ at time t after impact. Here v_b is the displacement velocity of the target surface due to impact. If the projectile and the target share the same impedance, then v_b is half the projectile velocity. V_p is the longitudinal (P) wave velocity, u is the particle displacement perpendicular to the boundary with respect to the unstrained position, and z is the collision direction (vertical for a falling block). Equation (C1) can be

readily derived: displacement of the boundary at time t after impact is given by $u = v_b \times t$. Away from the boundary, points will only start to move when the wave from the impact reaches them, at a time $t' = z/V_p$. The displacement at any point z will therefore be $u(z) = v_b \times (t - t') = v_b \left(t - \frac{z}{V_p} \right)$. This results in the displacement gradient $\frac{\partial u}{\partial z} = \frac{-v_b}{V_p}$.

Using positive compressive stress convention, the stress due to unidirectional compression along z is

$$\sigma_{zz} = -(\lambda + 2\mu) \frac{\partial u}{\partial z} = (\lambda + 2\mu) \frac{v_b}{V_p} \quad (C2)$$

And, in the absence of horizontal strain,

$$\sigma_{xx} = \sigma_{yy} = -\lambda \frac{\partial u}{\partial z} = \lambda \frac{v_b}{V_p} = \frac{\lambda}{\lambda + 2\mu} \sigma_{zz}, \quad (C3)$$

where λ , μ are Lamé's parameters for an isotropic elastic solid. Generation of fractures may then be diagnosed as a function of v_b using the two stress components and rock tension or shear fracturing stress, or, assuming pre-existing cracks, using material toughness values.

III.4. Matching traction and displacement for mixed media collision

We will treat the water-saturated sediment as a fluid with the properties of water. Matching traction and displacement continuity produces the well-known result that traction perpendicular to the impact boundary (σ_{zz} for the solid, pressure P for the water saturated sediment) will be the same, i.e. $\sigma_{zz} = P$. However, if the impedance of the block (projectile) and the sediment (target) are unequal, the boundary displacements with respect to unstrained conditions of either objects will be unequal. Therefore, instead of a unique boundary velocity v_b , we should define v_r as the boundary deflection with respect to the unstrained rock of the boulder, and v_w as the boundary deflection with respect to the unstrained sediment (note that v_r and v_w are in different kinematic referentials). In terms of wave propagation analysis, v_r corresponds to the reflected particle velocity inside the boulder, and v_w corresponds to the transmitted particle velocity in the sediment.

After impact (but before any rebound), the boundary will be joined, so we have to match the block falling velocity v_i and the respective boundary velocities in each medium referential such that: $|v_i| = |v_w| + |v_r|$ (Fig. III.1, lower diagram). Adopting a referential in each media which is pointing away from the boundary (positive z up in the block, positive z down in the sediment) and recalling that v_w , v_r are defined relative to the unstrained positions of both media, we can write $v_i = v_w + v_r$

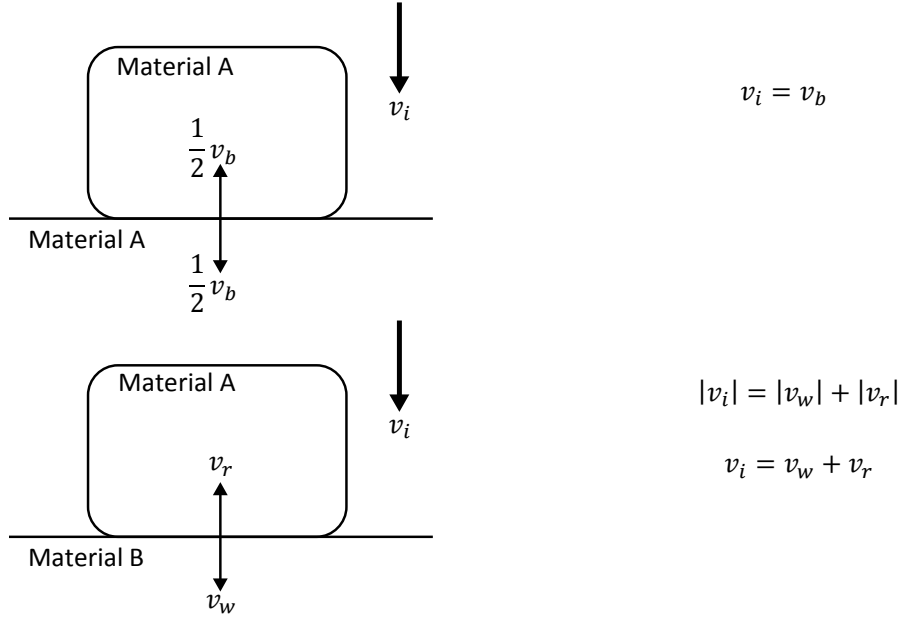


Figure III.1. Explanation of the boundary conditions between water saturated sediment and the gneiss block.

Proceeding in similar fashion as for equations (C2 and C3), we can equate pressure in the unconsolidated sediment to

$$P = K \frac{\partial u_z}{\partial z} = K \frac{v_w}{V_w} \quad (C4)$$

where K is water incompressibility (bulk modulus) and V_w is the pressure wave velocity in the water-saturated sediment. Now matching P and σ_{zz} for traction continuity, we obtain

$$P = \sigma_{zz} = \frac{K}{V_w} v_w = \frac{(\lambda + 2\mu)}{V_p} v_r \quad (C5)$$

This equates to

$$v_w Z_w = v_r Z_r \quad (C6)$$

where we define the specific impedances Z such that $Z_w = \sqrt{\rho_w K} = K/V_w$ and $Z_r = \sqrt{\rho_r (\lambda + 2\mu)} = \frac{\lambda + 2\mu}{V_p}$ and the wave velocities as $V_p = \sqrt{\frac{\lambda + 2\mu}{\rho_r}}$ and $V_w = \sqrt{\frac{K}{\rho_w}}$ where ρ_r and ρ_w are mass densities for rock and water respectively.

Using the $v_i = v_w + v_r$, equation (C5) and the impedances, we can now derive a direct relation between P and impact velocity v_i :

$$P = \sigma_{zz} = Z_w \frac{Z_r}{Z_r + Z_w} v_i = \frac{Z_w Z_r}{Z_r + Z_w} v_i$$

$$P = \frac{1}{\frac{Z_r}{Z_w Z_r} + \frac{Z_w}{Z_w Z_r}} v_i$$

$$P = \left(\frac{1}{Z_w} + \frac{1}{Z_r} \right)^{-1} v_i$$

If we now define the harmonic mean of the specific impedances as $\zeta = \frac{1}{2} \left(\frac{1}{Z_r} + \frac{1}{Z_w} \right)^{-1}$ we can write

$$\sigma_{zz} = P = 2\zeta v_i$$

$$\sigma_{xx} = \sigma_{yy} = \frac{\lambda}{\lambda + 2\mu} 2\zeta v_i \quad (C7)$$

III.5. Hydrofracturing criterion

Following impact, the block will compress in the vertical direction and want to expand in the horizontal direction. Immediately after impact, particles away from the edges of the block are confined by surrounding particles and are therefore unable to undergo this lateral extension, thereby setting up a horizontal stress that opposes extension. Extension first occurs at the edges of the block where the particles are unconfined, then migrates inwards. This means that the pressure required for hydrofracturing to occur should not only exceed the tensile strength of the gneiss, but also the horizontal stress. Hence if the dynamic tensile strength of gneiss is T , we can write as a hydrofracturing criterion

$$P > T + \sigma_{xx} \quad (C8)$$

which after substitution from equation (C7) results in

$$2\zeta v_i > \sigma_c + \frac{\lambda}{\lambda + 2\mu} 2\zeta v_i \quad (C9)$$

If we single out v_i we can now obtain an expression for the minimum impact velocity to generate hydrofracturing:

$$v_i = \frac{T}{2\zeta \left(1 - \frac{\lambda}{\lambda + 2\mu} \right)} \quad (C10)$$

Once the value of the initial velocity, v_i has been obtained, this value can be put into the free fall equation

$$v_i = \sqrt{2gh} \quad (\text{C11})$$

where h is the fall height and g is acceleration due to gravity, to determine the minimum height the block must fall from to provide a pressure great enough to overcome the tensile strength and the horizontal stress.

Appendix IV – Calculation results

Brazilian disc testing was used to find the tensile strength of the gneiss (Appendix V). This accounts for just one parameter required to ultimately calculate the fall height of the block. In addition, the shear modulus (μ), the first Lamé parameter (λ), and the P wave velocity (V_p) of the gneiss must be known, along with the acoustic wave velocity (V_w) and the bulk modulus (K) of the liquid substrate, here assumed to have the properties of water. The acoustic wave velocity of water is known to be 1500 m/s. A value of 2200 MPa for the bulk modulus of water was also easily obtained (Engineering ToolBox 2004).

Ascertaining the Lamé parameters of the gneiss has proved much more challenging, as it is typically only reported for rocks at depth. Ji *et al.* (2010) report a λ value for felsic-intermediate gneiss of 25 – 50 GPa at pressures of 600 MPa (20-25 km depth). This value decreases to 11 – 12 GPa at surface pressures (Ji *et al.* 2010, their figure 1c). μ is also reported for rocks at depth, and no sources were found that allowed a value to be extrapolated to surface pressures. Ji *et al.* (2010) give a μ/λ ratio of 1.057 for felsic rocks, or $\mu \approx \lambda$, supported by the trend of μ - λ plots in their figures 8 and 9. It was therefore decided to let $\mu = \lambda$.

This leaves the P-wave velocity of the gneiss. Once again, this value is reported in the literature for rocks at depth. Hall & Al-Haddad (1976) give a V_p value of 5.28 ± 0.23 km/s for the Lewisian gneiss in their ‘Boundary region’, the nearest location to Clachtoll. They also report a velocity gradient of ~ 0.1 km/s/km in the uppermost crust. Levander *et al.* (1994) report a V_p of 6.10 – 6.24 km/s corrected to 250 MPa at 140 °C, i.e. a depth of ~ 10 km. Using the velocity gradient of Hall and Al-Haddad (1976), this extrapolates to 5.10 – 5.24 km/s at the surface, though it may not be reasonable to assume that this gradient is linear. Christensen (1965) gives average velocities of 5.1 and 4.8 km/s for their gneiss samples 3 and 4 respectively – those which most closely resemble the Lewisian gneiss at Clachtoll in terms of mineralogy and grain size. They also report no clear relationship between P-wave velocity and P-wave direction relative to foliation orientation, effectively allowing us to assume the gneiss is seismically isotropic. Averaging the values obtained from these sources gives a P-wave velocity of 5.1 km/s.

Another way to obtain a P-wave velocity for the gneiss is to substitute the λ and μ values into the equation $V_p = \sqrt{\frac{\lambda+2\mu}{\rho}}$ using a ρ value of 2700 kg/m³.

$$\Rightarrow V_p = \sqrt{\frac{12GPa + 2 \times 12GPa}{2700}} = 3650 \text{ m/s}$$

Whilst significantly lower than the values in the literature, this does not seem unreasonable for a P-wave velocity at the surface when compared to the λ - V_p plots in Ji et al.'s (2010, their figure 6).

In the light of the above, we decided to perform the calculation twice, using V_p values of both 5100 m/s and 3650 m/s. λ , μ , K , V_p and V_w can be used to find Z_w and Z_r , where $Z_w = \frac{K}{V_w}$ and $Z_r = \frac{\lambda+2\mu}{V_p}$.

These values can be used to define the harmonic mean $\zeta = \frac{1}{2} \left(\frac{1}{Z_r} + \frac{1}{Z_w} \right)^{-1}$ and, once values are known for T (the tensile strength of the gneiss), to compute the impact velocity according to (C10): $v_i =$

$$\frac{T}{2\zeta \left(1 - \frac{\lambda}{\lambda+2\mu} \right)}$$

From v_i and the free-fall equation, we can compute the minimum height from which the block must have fallen. The results are shown in Table VI.1.

For a tensile strength of the gneiss of 9 MPa, and a V_p value of 3650 m/s, the minimum fall height is 5.7 m, or 6.3 m with a V_p of 5100 m/s. Ultimately, 6 m is a best estimate for the height from which the block must fall to generate sufficient overpressure to fracture the gneiss. Given the dimensions of the block, it also seems feasible that the block wouldn't significantly disaggregate over such a distance.

Table VI.1. Values of parameters (left side of table) required to calculate the impact velocity and fall height of the Clachtoll megablock (right side of table). Values of T were obtained using Brazilian Tests (see Appendix E).

T (MPa)	λ (MPa)	μ (MPa)	K (MPa)	V_p (m/s)	V_w (m/s)	Z_r (MPa s/m)	Z_w (MPa s/m)	ζ (MPa s/m)	v_i (m/s)	h (m)
6	12000	12000	2200	3650	1500	9.8630	1.4667	0.6384	7.0	2.5
7	12000	12000	2200	3650	1500	9.8630	1.4667	0.6384	8.2	3.5
8	12000	12000	2200	3650	1500	9.8630	1.4667	0.6384	9.4	4.5
9	12000	12000	2200	3650	1500	9.8630	1.4667	0.6384	10.6	5.7
10	12000	12000	2200	3650	1500	9.8630	1.4667	0.6384	11.7	7.0
11	12000	12000	2200	3650	1500	9.8630	1.4667	0.6384	12.9	8.5
12	12000	12000	2200	3650	1500	9.8630	1.4667	0.6384	14.1	10.1
6	12000	12000	2200	5100	1500	7.0588	1.4667	0.6072	7.4	2.8
7	12000	12000	2200	5100	1500	7.0588	1.4667	0.6072	8.6	3.8
8	12000	12000	2200	5100	1500	7.0588	1.4667	0.6072	9.9	5.0
9	12000	12000	2200	5100	1500	7.0588	1.4667	0.6072	11.1	6.3
10	12000	12000	2200	5100	1500	7.0588	1.4667	0.6072	12.4	7.8
11	12000	12000	2200	5100	1500	7.0588	1.4667	0.6072	13.6	9.4
12	12000	12000	2200	5100	1500	7.0588	1.4667	0.6072	14.8	11.2

Appendix V – Brazilian tests

Determining the fall height of the block using the free fall calculation requires the tensile strength of the gneiss as an input parameter. In order to ascertain the tensile strength of the specific gneiss from the Clachtoll Megablock, Brazilian disc tests were performed on a selection of cores, using the methodology outlined in Part 2 of Bieniawski & Hawkes (1978). The test measures the indirect uniaxial tensile strength of a specimen. Measuring the indirect strength is important for realistically modelling the impact event – it is the downward motion being impeded by impact that results in the opening of tensile fractures (indirect), rather than an active pulling apart of the block (direct).

E.1 - Experiment methodology

1. Apparatus

- (i) A pair of steel loading jaws intended to grip a disc-shaped specimen at diametrically-opposed surfaces (Fig. V.1).
- (ii) A machine appropriate for the application and measurement of compressive loads applied to the specimen, preferably with a fitted load/displacement recorder. Here, the biaxial loading apparatus in Durham University's Rock Mechanics Laboratory was utilised.
- (iii) A high speed camera was used to verify that rupture initiated in the centre of the specimen, not the perimeter. The latter would arise due to edge effects and wouldn't give a true tensile strength. In addition to the high speed camera, a bright lighting set-up is required to sufficiently illuminate the specimen, given the high frame rate of the camera.

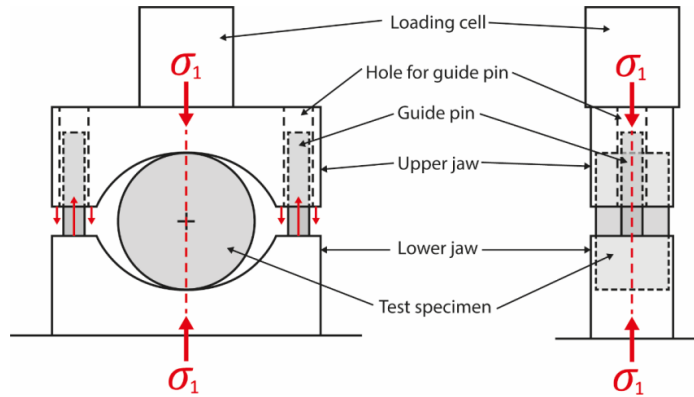


Figure V.1. Set-up for loading jaws, specimen and loading cell. Following Bieniawski and Hawkes (1978), the critical dimensions are: the radius of curvature of the jaws ($1.5 \times$ specimen radius); the clearance and length of the guide pins coupling the two jaws (they must not permit rotation of one jaw relative to the other out of plane by more than 4×10^{-3} rad); and the width of the jaws ($1.1 \times$ specimen thickness).

2. Specimens

A compositionally representative sample of the Lewisian gneiss was taken from the hillside approximately 100 m southeast of the CM. Four cores with a diameter of 20 mm were taken from the sample, two parallel to the foliation of the gneiss, and two perpendicular. These cores were then sliced to obtain discs with a thickness varying from 13 to 20 mm. In total, four discs were made with the axes of the core running parallel to foliation (P1-P4), and four perpendicular (O1-O4) (Fig. V.2. and Table V.1). The remaining core was designated ‘spare’. As required by the method detailed by Bieniawski & Hawkes (1978), the cylindrical surfaces were free from tool marks, and irregularities across the thickness of the specimen did not exceed 0.025mm. End faces were flat to within 0.25mm and square and parallel to within 0.25° .

Table V.1. Specimen orientations (relative to foliation in sample) and dimensions. Each specimen’s diameter and length were measured three times using digital callipers to calculate a mean value.

Specimen	Diam. 1 (mm)	Diam. 2 (mm)	Diam. 3 (mm)	Diam. Mean (mm)	Length 1 (mm)	Length 2 (mm)	Length 3 (mm)	Length Mean (mm)
P1	20.04	20.06	20.05	20.05	15.55	15.51	15.53	15.53
O1	19.97	19.98	19.99	19.98	20.89	20.91	20.90	20.90
P2	20.18	20.15	20.06	20.13	13.56	13.56	13.53	13.55
P4	20.05	20.02	20.07	20.05	18.95	18.89	18.93	18.92
P3	20.04	20.06	20.06	20.05	17.46	17.49	17.45	17.47
O2	19.99	19.98	19.99	19.99	14.42	14.43	14.43	14.43
O4	20.01	19.82	19.77	19.87	15.47	15.41	15.42	15.43
O3	19.99	19.99	19.99	19.99	13.13	13.11	13.17	13.14

3. Procedure

- (a) The test specimens were cut and prepared using clean water, then stored in a sealed plastic bag until use.
- (b) The loading jaws, with the first specimen in place were squarely positioned in the biaxial loading apparatus, such that the load was applied to the specimen diametrically (Fig. V.3). Upon inserting the specimen into the jaws, the orientation of its foliation relative to the loading direction was recorded (Fig. V.4).
- (c) The high speed camera and appropriate lighting were then set up and the camera focused.
- (d) A continuous load was then applied to each specimen in turn, at a constant rate, until failure occurred. The load/displacement recorder was used throughout to precisely determine the load at primary fracture.
- (e) After each test, the footage captured by the high speed camera was reviewed to ensure that the fracture nucleated in the centre of the specimen (Fig. V.6).

4. Conversion of results to tensile strength

The following formula is used to determine the tensile strength of the specimen:

$$\sigma_t = 0.636 F/Dt$$

Where σ_t is tensile strength, F is the load at failure (N), D is the diameter of the specimen (mm) and t is the thickness of the specimen (mm).

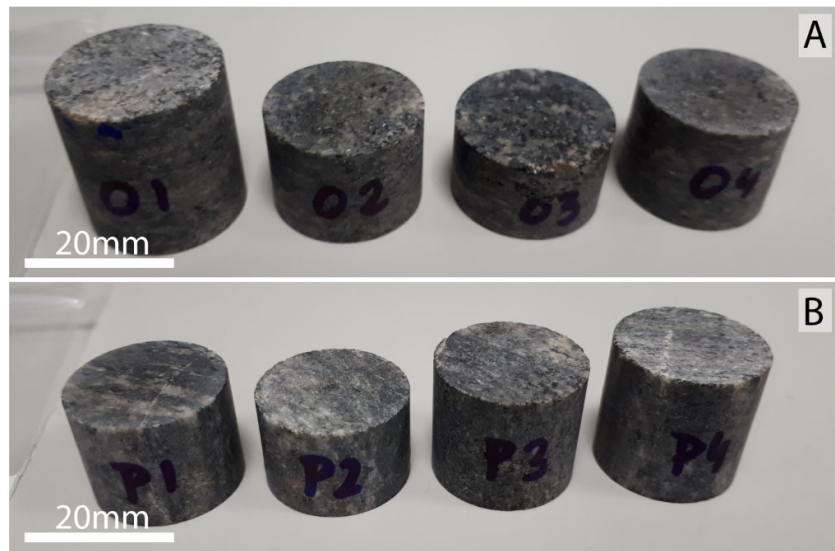


Figure V.2. Specimens prepared for testing. (a) Specimens O1 – O4, with cores cut orthogonal to foliation in gneiss – circular surface of cylinder displays plane of foliation; (b) Specimens P1 – P4, with cores cut parallel to foliation in gneiss – circular surface of cylinder cross-cuts foliation.

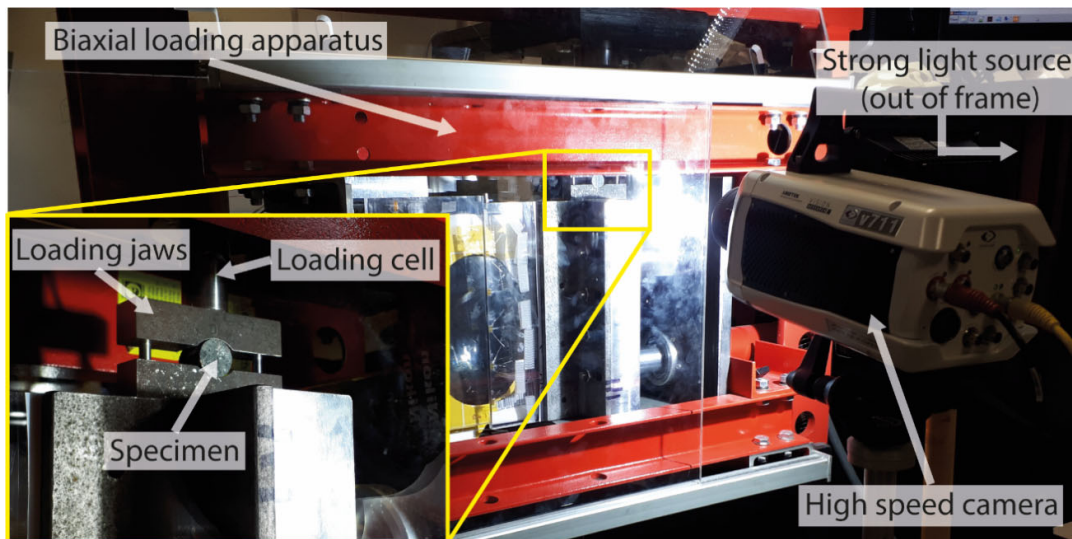


Figure V.3. Apparatus set-up for Brazilian test. Note that although the loading apparatus is capable of loading a specimen biaxially, this is unnecessary for performing a Brazilian test, and the specimens were only uniaxially loaded.

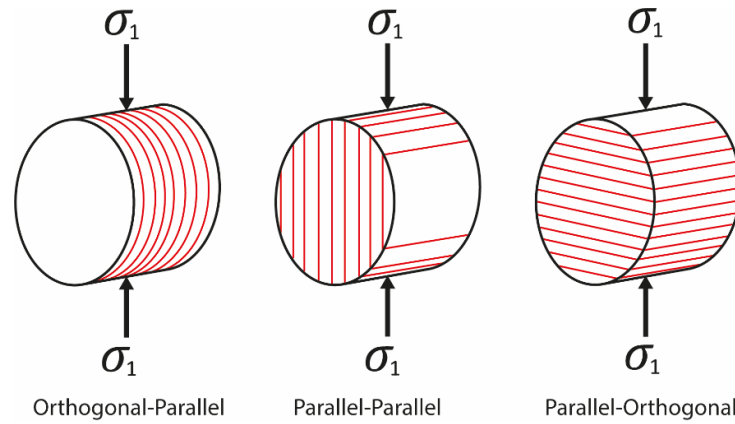


Figure V.4. Specimen loading orientations. Orientations are noted in two parts, each part of which can either be parallel or orthogonal. The first part refers to the orientation of the foliation with respect to the core cutting direction of the sample, whilst the second part refers to the orientation of the foliation with respect to the loading direction. Thus specimens O1 – O4 are all designated Orthogonal-Parallel, whilst samples P1 – P4 can either be loaded such that they are Parallel-Parallel or Parallel-Orthogonal.

V.2 - Results

1. Calibration

Prior to testing of the specimens, a known load was applied to the loading cell and jaws and the resulting voltage recorded so that a slope for load vs volts could be calculated (Fig. V.5). This relationship can then be used to ascertain the load for each test, given the voltage recorded at failure.

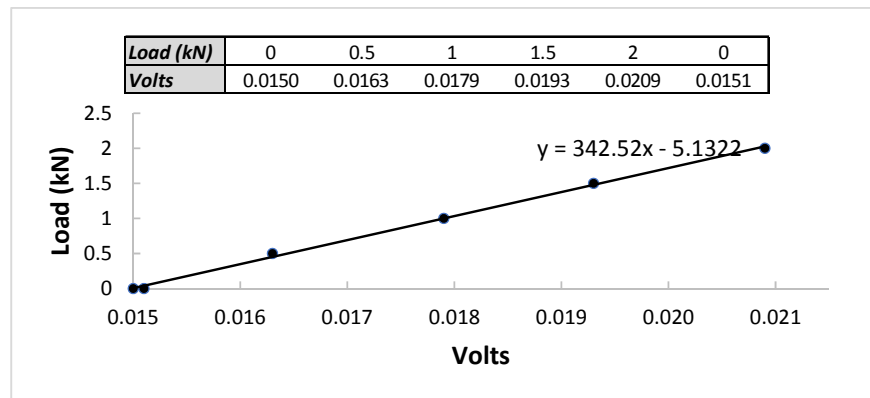


Figure V.5. Experiment calibration, applying a load of 0 to 2 kN at 0.5 kN intervals yielded a slope of 342.52.

2. Verification of initial fracture rupture location

To be sure that a true tensile strength was found, it was necessary to verify that a Mode I fracture nucleated in the centre of the test specimen. In order to do this, the high speed camera footage was carefully reviewed after each test to identify the location of fracture nucleation. An example of images from this process, for each of the three possible specimen orientations, is shown in Figure V.6. Example (A) is of interest because it contains a pre-existing weakness oriented approximately perpendicular to both the foliation and the loading direction. Fracturing did initially occur in the centre of the specimen, but was immediately followed by fracturing around the edges of the sample, in the vicinity of, and parallel to this existing weakness.

Also of note, was the difference in the fracture sets generated in specimen P1 and P4. Both specimens were oriented parallel-parallel, but whilst P1 failed along multiple parallel fractures, P4 failed along one, centrally located, discrete fracture (Fig. V.7). Inspection of the specimens indicates that this difference in failure behaviour is likely due to the relative abundance of micaceous minerals in P1, defining numerous planes of anisotropy when compared to P4.

3. Results and conversion to force and stress

The initial results of the Brazilian tests are shown in Table V.2. Two steps were required to convert these results to tensile strength. The first step uses the results of the experiment calibration to convert the recorded voltages to force, using the following equation (multiplying by 10^3 converts from kN to N):

$$F = slope \times (peakV - zeroV) \times 10^3$$

The second step uses the equation outlined in the experimental methodology to convert from force to stress:

$$\sigma = 0.636 F/Dt$$

The load vs time graphs recorded during the tests are presented in Figure V.8. The variable responses observed in the stress drop curves are considered to be a result of heterogeneities in fabric spacing, mineral modalities and grain size within the specimens, rather than being due to specimen orientation or experimental effects. It is expected that with a larger sample size, patterns would emerge that would more clearly identify variable responses in relation to the specimen orientation.

In some cases, after an initial stress drop, taken as the point of failure, stress then continues to rise. This is to be expected, given that the specimen should theoretically fail along its weakest layer. It then follows that the resulting two halves will each then individually be stronger than the original whole, having eliminated the weakest layer.

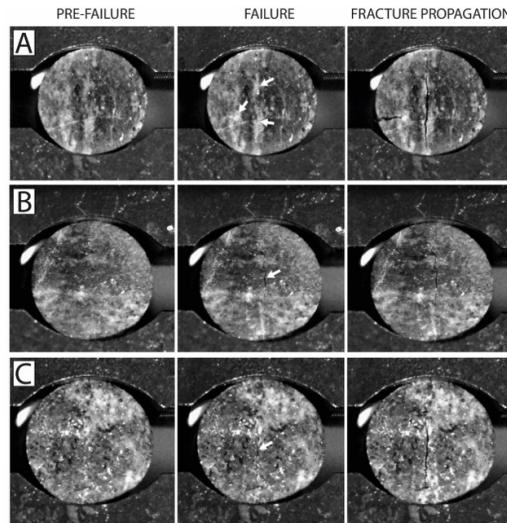


Figure V.6. High speed camera stills of fracture initiation. (A) shows an example of fracture initiation in a parallel-parallel oriented specimen, (B) a parallel-orthogonal oriented specimen, and (C) an orthogonal-parallel oriented specimen. The first column shows the specimens in their pre-failure state. The second column shows the frame recorded in which fracturing is first observed, denoted by the white arrows. Here, specimen (A) has three white arrows, highlighting a diffuse whitening of the sample in specific localities which then formed obvious fractures in one frames time (column 3).

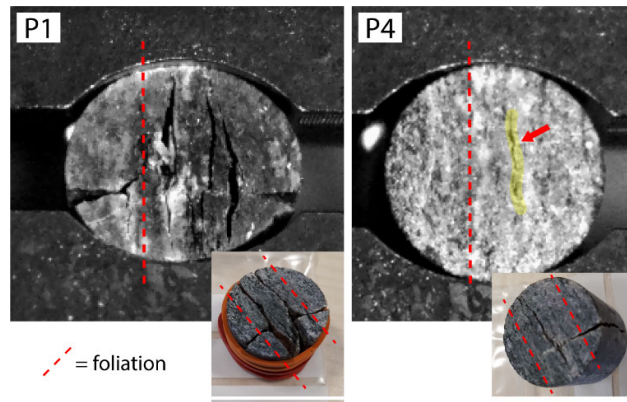


Figure V.7. High speed camera stills of fracture development in specimens P1 and P4, along with photos of the specimens after the experiment. P1 clearly shows fracturing along numerous parallel fractures, whilst P4 failed along one main foliation parallel fracture.

Table V.2. Brazilian test results. // denotes a parallel-parallel specimen orientation, T a parallel-orthogonal orientation, and – an orthogonal-parallel orientation.

Experiment #	Video file name	Specimen	Orientation	Diam. Mean (mm)	Length Mean (mm)	Zero V (V)	Peak V (V)	Force (N)	Stress (Mpa)
1	Z01	P1	//	20.05	15.53	0.0131	0.0177	1575.58	3.21566
2	Z02	O1	-	19.98	20.90	0.0164	0.0296	4521.24	6.89284
3	Z03	P2	T	20.13	13.55	0.0148	0.0231	2842.90	6.60751
4	Z04	P4	//	20.05	18.92	0.0124	0.0236	3836.20	6.42148
5	Z05	P3	T	20.05	17.47	0.0136	0.029	5274.78	9.58781
6	Z06	O2	-	19.99	14.43	0.0135	0.0331	6713.35	14.81216
7	-	O4	-	19.87	15.43	0.0138	0.0211	2500.38	5.13719
8	Z07	O3	-	19.99	13.14	0.0144	0.0273	4418.48	10.70663

The mean tensile strength was calculated for each of the three possible specimen orientations (Table V.3).

As expected, the parallel-parallel specimens had the lowest tensile strength, being optimally oriented to form fractures parallel to foliation. The orthogonal-parallel specimens are, in our view, the most accurate representation of the CM, with fractures forming parallel to the maximum principal stress, but orthogonal to the foliation. It was therefore initially decided to input this measurement into the fall height calculation. However, given the similarity in mean tensile strength of the orthogonal-parallel and parallel-orthogonal specimens, and their overlap when considering error, it was decided to group these specimen orientations so that a result could be used that derived from a larger sample size.

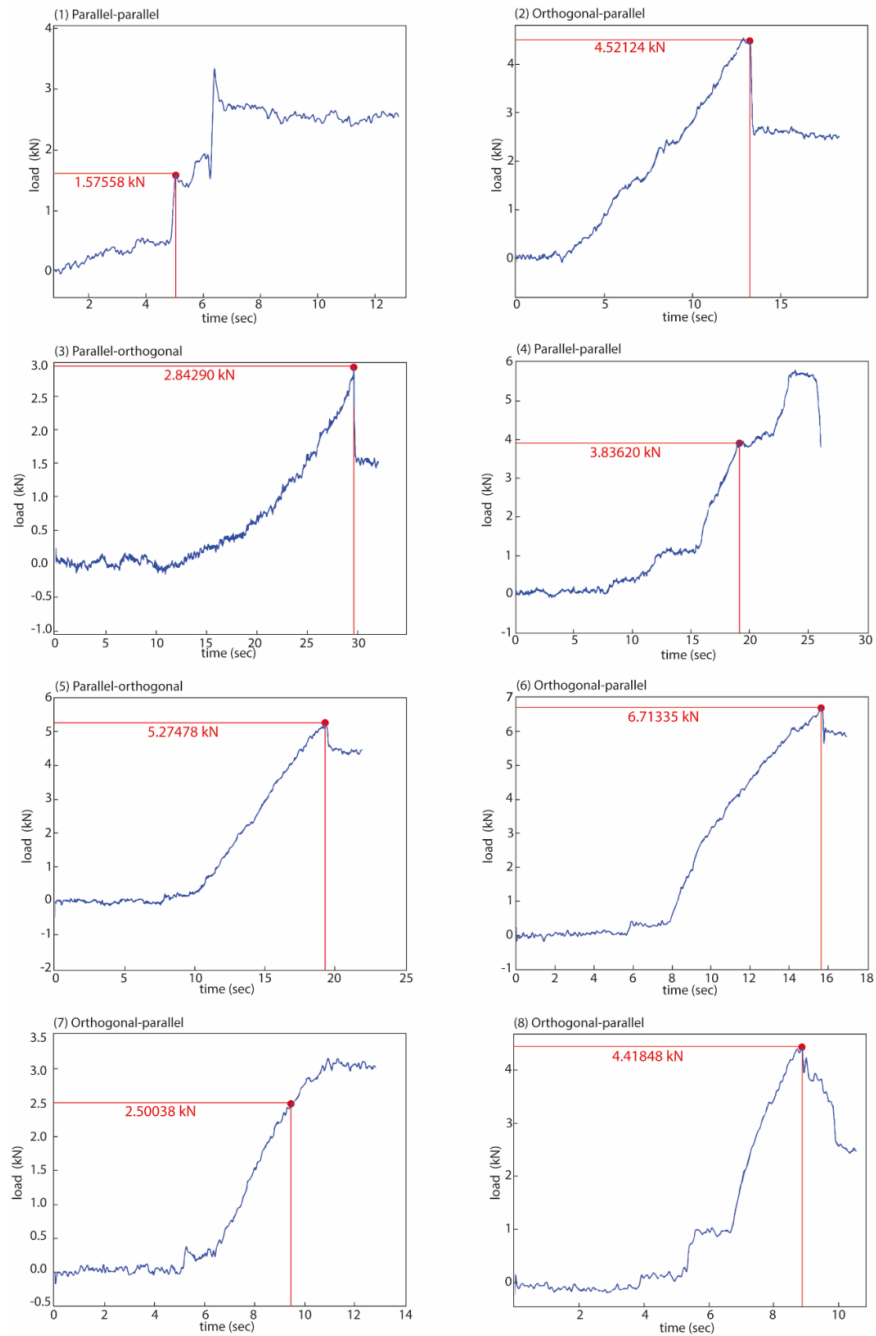


Figure V.8. Stress drop curves for each test. Red dots indicate failure of the specimen. Both parallel-parallel specimens showed relatively minor stress drops at failure. The parallel-orthogonal specimens showed more obvious stress drops, whilst the orthogonal-parallel specimens were much more variable in their behaviour.

Table V.3. Mean tensile strength calculations.

Specimen	Stress	//	T	-	T and -
P1	3.21566	✓			
O1	6.89284			✓	✓
P2	6.60751		✓		✓
P4	6.42148	✓			
P3	9.58781		✓		✓
O2	14.81216			✓	✓
O4	5.13719			✓	✓
O3	10.70663			✓	✓
Mean σ (Mpa)		4.8186	8.0977	9.3872	8.9574
Standard deviation		2.26685	2.10739	4.29944	3.52460
Mean tensile strength (MPa)		5 ± 2	8 ± 2	9 ± 4	9 ± 3

Additional References cited in Appendices I-V

Bieniawski, Z.T. and Hawkes, I. 1978. Suggested methods for determining tensile strength of rock materials. *Int. J. Rock Mech. Min. Sci. & Geomech. Abstr.* 15, 99–103.

Christensen, N.I. 1965. Compressional wave velocities in metamorphic rocks at pressures to 10 kilobars. *Journal of Geophysical Research*, 70 (24), 6147–6164.

<https://doi.org/10.1029/JZ070i024p06147>

Hall, J. and Al-Haddad, F.M. 1976. Seismic velocities in the Lewisian metamorphic complex, northwest Britain—‘in situ’ measurements. *Scottish Journal of Geology*, 12, 305–314.

<https://doi.org/10.1144/sjg12040305>

Engineering ToolBox (2004) Bulk Modulus and Fluid Elasticity. [Online]. 2004.

https://www.engineeringtoolbox.com/bulk-modulus-elasticity-d_585.html

Ji, S., Sun, S., Wang, Q. and Marcotte, D. 2010. Lamé parameters of common rocks in the Earth’s crust and upper mantle. *Journal of Geophysical Research: Solid Earth*. 115 (B6).

<https://doi.org/10.1029/2009JB007134>

Levander, A., Hobbs, R.W., Smith, S.K., England, R.W. 1994. The crust as a heterogeneous “optical” medium, or “crocodiles in the mist”. *Tectonophysics*, 232 (1), 281–297. [https://doi.org/10.1016/0040-1951\(94\)90090-6](https://doi.org/10.1016/0040-1951(94)90090-6)